Received: 7 August 2023 | Revised: 8 December 2023 | Accepted: 23 January 2024

DOI: 10.1111/adb.13381

ORIGINAL ARTICLE

Addiction Biology SSA WILEY

Cortical and subcortical microstructure integrity changes after repetitive transcranial magnetic stimulation therapy in cocaine use disorder and relates to clinical outcomes

Jalil Rasgado-Toledo[1] | Victor Issa-Garcia[1,2] | Ruth Alcalá-Lozano[3] | Eduardo A. Garza-Villarreal[1] | Gabriel González-Escamilla[4]

[1]Instituto de Neurobiología, Universidad Nacional Autónoma de México campus Juriquilla, Querétaro, Mexico

[2]Escuela de Medicina y Ciencias de la Salud TecSalud, Tecnológico de Monterrey, Monterrey, Mexico

[3]Laboratorio de Neuromodulación, Subdirección de Investigaciones Clínicas, Instituto Nacional de Psiquiatría "Ramón de la Fuente Muñíz", Mexico City, Mexico

[4]Department of Neurology, Focus Program Translational Neuroscience (FTN), Rhine-Main Neuroscience Network (rmn^2), University Medical Center of the Johannes Gutenberg University Mainz, Mainz, Germany

Correspondence

Eduardo A. Garza-Villarreal, Instituto de Neurobiología, Laboratorio B-03, Universidad Nacional Autonoma de Mexico (UNAM) campus Juriquilla, Boulevard Juriquilla 3001, Santiago de Querétaro, Querétaro 76230, Mexico.
Email: egarza@comunidad.unam.mx

Gabriel González-Escamilla, Department of Neurology, Focus Program Translational Neuroscience (FTN), Rhine-Main Neuroscience Network (rmn^2), University Medical Center of the Johannes Gutenberg University Mainz, Langenbeckstrasse 1, 55131 Mainz, Germany.
Email: ggonzale@uni-mainz.de

Ruth Alcalá-Lozano, Psychiatrist and Clinical Research, Instituto Nacional de Psiquiatría Ramon de la Fuente Muñiz, Laboratorio de Neuromodulación, Subdireccion de Investigaciones Clínicas, Calzada México Xochimilco 101, Colonia San Lorenzo Huipulco, Mexico City 14370, Mexico.
Email: ruthalcalalozano@gmail.com

Abstract

Cocaine use disorder (CUD) is a worldwide public health condition that is suggested to induce pathological changes in macrostructure and microstructure. Repetitive transcranial magnetic stimulation (rTMS) has gained attention as a potential treatment for CUD symptoms. Here, we sought to elucidate whether rTMS induces changes in white matter (WM) microstructure in frontostriatal circuits after 2 weeks of therapy in patients with CUD and to test whether baseline WM microstructure of the same circuits affects clinical improvement. This study consisted of a 2-week, parallel-group, double-blind, randomized controlled clinical trial (acute phase) (sham [$n = 23$] and active [$n = 27$]), in which patients received two daily sessions of rTMS on the left dorsolateral prefrontal cortex (lDLPFC) as an add-on treatment. T1-weighted and high angular resolution diffusion-weighted imaging (DWI-HARDI) at baseline and 2 weeks after served to evaluate WM microstructure. After active rTMS, results showed a significant increase in neurite density compared with sham rTMS in WM tracts connecting lDLPFC with left and right ventromedial prefrontal cortex (vmPFC). Similarly, rTMS showed a reduction in orientation dispersion in WM tracts connecting lDLPFC with the left caudate nucleus, left thalamus, and left vmPFC. Results also showed a greater reduction in craving Visual Analogue Scale (VAS) after rTMS when baseline intra-cellular volume fraction (ICVF) was low in WM tracts connecting left caudate nucleus with substantia nigra and left pallidum, as well as left thalamus with substantia nigra and left pallidum. Our results evidence rTMS-induced WM microstructural changes in fronto-striato-thalamic circuits and support its efficacy as a therapeutic tool in treating CUD. Further, individual clinical improvement may rely on the patient's individual structural connectivity integrity.

Jalil Rasgado-Toledo and Victor Issa-Garcia contributed equally.

Eduardo A. Garza-Villarreal and Gabriel González-Escamilla shared senior authorship.

Funding information
CONACYT FOSISS, Grant/Award Number: 0260971; CONACYT, Grant/Award Numbers: 253072, 858667; PAPIIT-UNAM, Grant/Award Number: IA202120; Dirección General de Calidad y Educación en Salud, Secretaría de Salud, México; German Research Foundation, Grant/Award Number: CRC-TR-128

KEYWORDS
addiction, cocaine use disorder, diffusion, MRI, NODDI, transcranial magnetic stimulation

1 | INTRODUCTION

Cocaine use disorder (CUD) is estimated to affect about 20 million people worldwide (global population age ≥15)[1] and is one of the leading causes of death in young people.[2] CUD induces pathological changes in the macrostructure and microstructure of the meso-cortico-limbic system in humans and animal models, possibly due to the changes in synapses and cells,[3] which may be reversible.[4] Despite the improvement in the treatment of CUD patients in recent years, patients with psychosocial and pharmacological approaches achieve only low to moderate effects on clinical symptomatology such as craving, which may lead to a relapse.[5] Novel non-invasive interventions such as repetitive transcranial magnetic stimulation (rTMS) have gained attention by attaining positive outcomes in substance use disorders (SUDs).[6] Although the main action mechanism of rTMS remains to be fully elucidated, the stimulation seems to induce acute modulation of the dysregulated frontostriatal circuits, and it is hypothesized that long treatments may produce neuroplastic changes in these circuits.[6,7] In this sense, rTMS may help patients adequately overcome symptoms such as craving and impulsivity by producing changes in micro- and macroscopic brain circuits.[7,8] We recently showed that rTMS at 5 Hz over the left dorsolateral prefrontal cortex (lDLPFC) reduced craving and impulsivity in CUD patients after 2 weeks and increased functional connectivity between lDLPFC and ventromedial prefrontal cortex (vmPFC), as well as vmPFC and right angular gyrus (AngG). However, to date, there is limited evidence on the extent to which rTMS modulates the microstructure of brain circuits in CUD.

Magnetic resonance imaging (MRI) has opened new opportunities for the study of microstructural abnormalities, these include the neurite orientation dispersion (OD) and density imaging model (NODDI), which allows the evaluation of subtle tissue characteristics by modelling water diffusion within neurites and the free water around them.[9] Microstructural metrics include (1) intra-cellular volume fraction (ICVF) or neurite density index, which assesses the density of axons and dendrites and has been proposed as a sensitive marker for myeloarchitecture and axonal degeneration; (2) isotropic volume fraction (ISOVF) which measures the free water of extracellular compartment as an indirect metric for neuroinflammation; and (3) OD index which quantifies bending, fanning and the orientational configuration of axons that helps to measure axonal organization.[10,11] Using NODDI offers an opportunity to understand rTMS treatment for CUD. This may be particularly interesting as NODDI could be developed into an indicator of a state-of-disorder and treatment-outcome biomarker.[12–14]

In this study, we wished to evaluate whether rTMS induces changes in white matter (WM) microstructure of brain circuits, related to substance abuse, after 2 weeks of rTMS treatment in CUD patients and to test whether baseline WM microstructure of those circuits could predict clinical improvement. To achieve this, we used longitudinal multi-shell diffusion-weighted imaging and NODDI analysis.

2 | METHODS

2.1 | Participants

Data were obtained from a clinical trial conducted at the Clinical Research Division of the National Institute of Psychiatry in Mexico City, Mexico, which was approved by the Institutional Ethics Research Committee (CEI/C/070/2016), registered at ClinicalTrials.gov (NCT02986438), and acquired as part of the SUDMEX-TMS database.[15] Detailed recruitment information, a CONSORT flowchart, and a complete demographics table, as well as the main clinical and fMRI study results, can be found in Angeles-Valdez et al.,[15] our previous publication by Garza-Villarreal et al.[16] and some details in the Supporting Information. During the clinical trial, patients with CUD who met the inclusion and did not meet exclusion criteria provided written informed consent to participate, per the Declaration Helsinki. Patients were recruited via flyers on SUD clinics and medical institutes in the metropolitan area of Mexico City and through advertisements on social media. The clinical trial consisted of a 2-week, parallel-group, double-blind, randomized controlled trial (acute phase) followed by a 6-month open-label trial (maintenance phase). rTMS was delivered over the lDLPFC as an add-on to standard treatment (full information can be found in the Supporting Information). Clinical, behavioural, and MRI data were acquired at baseline (T0), 2 weeks (T1), 3 months (T2), and 6 months (T3). The main results of the clinical trial and functional analysis results have been published.[16] For this new study, we focused on the double-blind 2-week acute phase (T0–T1) and the relationship between clinical improvement and WM structure measured using a novel high angular resolution diffusion-weighted imaging (DWI-HARDI)

sequence and NODDI analysis. We analysed 50 participants (sham: 23, active: 27), and the overview of demographic data is shown in Table 1.

2.2 | Clinical instruments

Table 1 shows the clinical instruments. A full list with their descriptions and mean scores can be found in Garza-Villarreal et al.[16] Here, we limit to describe the following which were employed in the analyses.

2.2.1 | Cocaine craving Visual Analogue Scale (VAS)

We designed a VAS to evaluate the participants' cravings at the moment of the assessment. The VAS consisted of a continuous 10 cm line (including two decimals) in which the left point at 0 cm meant 'no craving' and the right point at 10 cm meant 'the most intense craving'.[17] The participants were asked to mark with a cross the intensity of their craving at the moment of assessment.

2.2.2 | Cocaine Craving Questionnaire Now (CCQ-now)

The CCQ-Now is a questionnaire containing 45 items that explore cocaine craving at the moment of assessment.[18] The items are related to the desire to use cocaine, the intention and planning to use cocaine, the anticipation of a positive outcome, the anticipation of relief from withdrawal or dysphoria, and the lack of control overuse. The higher the score is, the higher the current cocaine craving. We employed the CCQ-now Spanish translation which was validated in the Mexican population.[19]

2.2.3 | Barratt Impulsivity Scale Version 11 (BIS-11)

The BIS is more than 50 years old and has been extensively revised into the BIS-11.[20] This version of the scale consists of 30 items that describe impulsive and non-impulsive behaviours related to three main categories: attentional, motor, and non-planning impulsiveness. The higher the total score is, the higher the impulsivity of the participant. We used the Spanish translation of the BIS-11.[21]

2.3 | Transcranial magnetic stimulation

During the acute phase, a MagPro R30+Option magnetic stimulator and an eight-shaped B65-A/P coil (MagVenture, Alpharetta, GA) were used to deliver active or sham rTMS over the lDLPFC. The orientation of the coil was anterior-medial, and the position was determined using either the 5.5 cm anatomic criterion or the Beam F3 method. The stimulation protocol consisted of 10 weekdays of two sessions with 50 trains of 50 pulses at 5 Hz at 100% motor threshold. Each train had a 10-s inter-train interval and each session had a 15-min inter-session interval. A total of 5000 pulses were delivered per day. For all details on the rTMS protocol, please refer to the Supporting Information.

2.4 | Simulation of TMS electrical field

We used SimNIBS[22] version 3.2.3 to perform simulations of the TMS electrical field generated on the participant's cortex. We reconstructed head meshes from T1-weighted (T1w) images using *headreco*.[23] During the study, Brain Navigator was not available; hence, a vitamin E capsule fiducial was used to identify the stimulation target. These scalp coordinates were projected into the cortex and converted to MNI coordinates reported in and with a procedure explained in detail in Garza-Villarreal et al.[16] We converted these MNI coordinates into the native space by using SimNIBS's *mni2subjects_coords* function which were projected back into the scalp before running the subjects' simulations. Simulations were run with the corresponding coordinates, coil orientation (anterior-medial), and 100% motor threshold. For the simulation, we used the MagVenture_MC_B70 (MCF-B70) coil, because there are no differences in the induced field between the B65-A/P and the MCF-B70 coil. Electric-field norms from simulations were mapped into *fsaverage* and then averaged across participants to obtain Figure 1.

2.5 | MRI acquisition

T1w and DWI-HARDI sequences were acquired using a Philips Ingenia 3 T scanner (Philips, USA) with a 32-channel Philips head coil. Parameters of T1w 3D FFE sagittal images were TR/TE = 7/3.5 ms, FA = 8°, FOV = 240 mm^2, matrix = 240 × 240, voxel = 1 × 1 × 1 mm, gap = 0. DWI-HARDI used a spin echo (SE) sequence, TR/TE = 9000/127 ms, FOV = 230 mm^2 (for four participants = 224 mm^2), matrix = 96 × 96 (for four participants = 112 × 112), number of slices = 57 (for four participants = 58), gap = 0, plane = axial, voxel = 2.4 × 2.4 × 2.5 mm (for four participants = 2 × 2 × 2.3 mm), directions: 8 = b0, 32 = *b* value 1000 s/mm^2 and 96 = *b* value 2500 s/mm^2 (for four participants: 96 = *b* value 3000 s/mm^2), total = 136 directions. Field maps intended for DWI-HARDI use were acquired using a SE-EPI sequence with the following parameters: TR/TE = 9000/127 ms, flip angle = 90°, matrix = 128 × 128 (for four participants = 112 × 112), voxel size = 1.8 × 1.8 × 2.5 mm (for four participants = 2 × 2 × 2.3 mm), number of slices = 57 (for four participants = 58), phase encoding direction = PA. A total of seven b0 volumes were acquired. Quality control (QC) of the T1w and DWI-HARDI images are described in the data report of SUDMEX-TMS,[15] using EDDY_QC to extract QC metrics sensitive and specific to artefacts, besides a visual inspection before and after preprocessing step ensuring good quality and the reliability of the included data and performed analyses.

TABLE 1 Descriptive statistics of demographics, behavioural instruments, and NODDI metrics by time point and sham/active groups.

	Sham		Active	
	T0 ($n = 23$)	T1 ($n = 20$)	T0 ($n = 30$)	T1 ($n = 25$)
Demographic				
Sex, *n* (%)				
Male	20 (87%)	-	25 (83.3%)	-
Female	3 (13%)	-	5 (16.7%)	-
Age in years, mean ± SD	33.3 ± 8.1	-	36.1 ± 6.8	-
Years of education, mean ± SD	13.4 ± 2.8	-	12.9 ± 3.1	-
Behavioural instrument, mean ± SD				
Craving: VAS	2.9 ± 2.9	2.3 ± 2.5	3.7 ± 3.5	1.5 ± 2.4
Craving: CCQ-now	146 ± 47.8	129.2 ± 46.2	148.7 ± 51.5	114.8 ± 44.7
Impulsivity: BIS-11	62.6 ± 16.9	59.8 ± 21.4	65 ± 16.6	53.4 ± 17.1
NODDI metrics, mean ± SD	**T0 ($n = 23$)**	**T1 ($n = 20$)**	**T0 ($n = 27$)**	**T1 ($n = 23$)**
ICVF: Caud2Medulla	0.812 ± 0.056	0.814 ± 0.063	0.813 ± 0.053	0.825 ± 0.066
ICVF: Caud2Palli	0.818 ± 0.061	0.815 ± 0.066	0.818 ± 0.056	0.823 ± 0.065
ICVF: DLPFC2Caud	0.631 ± 0.076	0.624 ± 0.073	0.627 ± 0.051	0.639 ± 0.063
ICVF: DLPFC2rvmPFC	0.515 ± 0.129	0.477 ± 0.1	0.451 ± 0.116	0.484 ± 0.126
ICVF: DLPFC2Thal	0.676 ± 0.068	0.673 ± 0.071	0.676 ± 0.038	0.686 ± 0.056
ICVF: rAngG2rDLPFC	0.663 ± 0.066	0.668 ± 0.073	0.674 ± 0.036	0.674 ± 0.045
ICVF: Thal2Medulla	0.757 ± 0.08	0.761 ± 0.081	0.759 ± 0.06	0.773 ± 0.072
ICVF: Thal2Palli	0.771 ± 0.067	0.775 ± 0.07	0.776 ± 0.058	0.784 ± 0.066
ICVF: vmPFC2DLPFC	0.476 ± 0.126	0.441 ± 0.1	0.422 ± 0.135	0.461 ± 0.142
ICVF: CCforcepsMajor	0.902 ± 0.071	0.891 ± 0.087	0.93 ± 0.045	0.925 ± 0.064
ISOVF: Caud2Medulla	0.298 ± 0.068	0.296 ± 0.077	0.336 ± 0.072	0.333 ± 0.085
ISOVF: Caud2Palli	0.212 ± 0.064	0.214 ± 0.07	0.247 ± 0.067	0.249 ± 0.076
ISOVF: DLPFC2Caud	0.178 ± 0.057	0.175 ± 0.059	0.192 ± 0.042	0.192 ± 0.04
ISOVF: DLPFC2rvmPFC	0.288 ± 0.078	0.287 ± 0.086	0.281 ± 0.084	0.283 ± 0.086
ISOVF: DLPFC2Thal	0.219 ± 0.055	0.217 ± 0.061	0.242 ± 0.046	0.242 ± 0.05
ISOVF: rAngG2rDLPFC	0.143 ± 0.038	0.149 ± 0.043	0.164 ± 0.032	0.163 ± 0.035
ISOVF: Thal2Medulla	0.393 ± 0.09	0.388 ± 0.101	0.434 ± 0.071	0.431 ± 0.081
ISOVF: Thal2Palli	0.313 ± 0.079	0.313 ± 0.086	0.348 ± 0.075	0.349 ± 0.082
ISOVF: vmPFC2DLPFC	0.144 ± 0.047	0.139 ± 0.049	0.138 ± 0.048	0.147 ± 0.049
ISOVF: CCforcepsMajor	0.503 ± 0.087	0.487 ± 0.090	0.523 ± 0.132	0.506 ± 0.108
OD: Caud2Medulla	0.378 ± 0.041	0.373 ± 0.047	0.398 ± 0.044	0.393 ± 0.052
OD: Caud2Palli	0.355 ± 0.028	0.351 ± 0.028	0.362 ± 0.033	0.362 ± 0.037
OD: DLPFC2Caud	0.423 ± 0.041	0.411 ± 0.031	0.41 ± 0.037	0.416 ± 0.035
OD: DLPFC2rvmPFC	0.399 ± 0.073	0.391 ± 0.083	0.365 ± 0.093	0.381 ± 0.094
OD: DLPFC2Thal	0.421 ± 0.037	0.411 ± 0.03	0.418 ± 0.03	0.42 ± 0.027
OD: rAngG2rDLPFC	0.415 ± 0.024	0.405 ± 0.019	0.413 ± 0.027	0.411 ± 0.024
OD: Thal2Medulla	0.429 ± 0.064	0.423 ± 0.072	0.455 ± 0.049	0.446 ± 0.053
OD: Thal2Palli	0.413 ± 0.04	0.407 ± 0.044	0.426 ± 0.034	0.423 ± 0.037
OD: vmPFC2DLPFC	0.347 ± 0.093	0.327 ± 0.089	0.294 ± 0.095	0.329 ± 0.096
OD: CCforcepsMajor	0.138 ± 0.053	0.141 ± 0.069	0.142 ± 0.028	0.14 ± 0.027

Note: Sample Size/Mean (percentage/±standard deviation) for demographics and NODDI metrics for each tract.

Abbreviations: VAS, visual analog scale; CCQ-now, cocaine craving questionnaire now version; BIS-11, Barrat impulsivity scale version 11; NODDI, neurite orientation dispersion and density imaging model; ICVF, intra-cellular volume fraction; ISOVF, isotropic volume fraction; SD, standard deviation; *n*, sample

size; OD, orientation dispersion; T0, baseline; T1, after 2 weeks; White matter (WM) regions of interest (ROI): Caud2Medulla, WM connecting left caudate nucleus and axial section through medulla; Caud2Palli, WM connecting left caudate nucleus and left pallidum; DLPFC2Caud, WM connecting left rostral middle frontal cortex (RMFC) and left caudate nucleus; DLPFC2rvmPFC, WM connecting left RMFC and right medial orbitofrontal cortex (MOC); DLPFC2Thal, WM connecting left RMFC and left thalamus; rAngG2rDLPFC, WM connecintg right inferior parietal cortex and right RMFC; Thal2Medulla, WM connecting left thalamus and left pallidum; Thal2Palli, WM connecting left thalamus and left pallidum; vmPFC2DLPF, WM connecting left MOC and left RMFC; CCforcepsMajor, forceps major of corpus callosum (control WM).

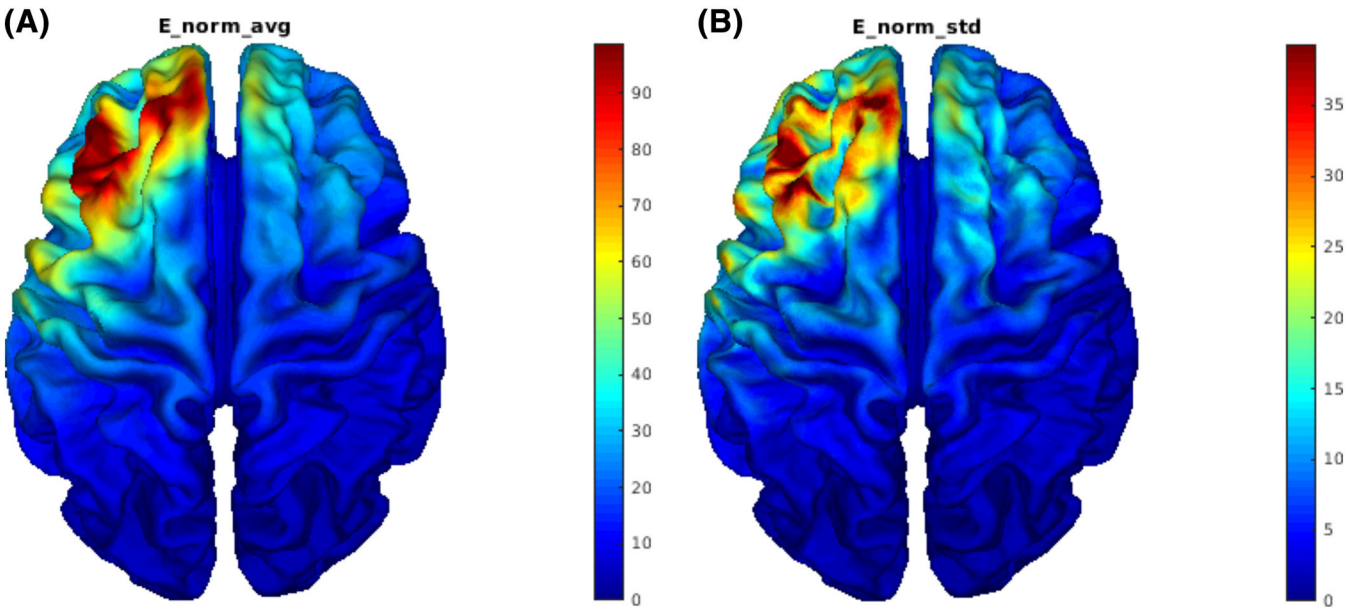

FIGURE 1 Visualization of (A) mean (V/m) and (B) standard deviation (V/m) of electric-field norms from simulations across subjects.

2.6 | Preprocessing

T1w preprocessing was performed using FMRIPREP v1.5.5[24] (RRID:SCR_016216), a Nipype-based tool[25] (RRID:SCR_002502). Each T1w volume was corrected for intensity non-uniformity (INU) using N4BiasFieldCorrection v2.1.0[26] and skull-stripped using *antsBrainExtraction.sh* v2.1.0 (using the OASIS template). Brain surfaces were reconstructed using *recon-all* from FreeSurfer v6.0.1[27] (RRID:SCR_001847), and the brain mask estimated previously was refined with a custom variation of the method to reconcile ANTs-derived and FreeSurfer-derived segmentations of the cortical grey matter (GM) of Mindboggle[28] (RRID:SCR_002438).

DWI-HARDI preprocessing was performed in MRtrix version 3.0_RC3,[29] using an established pipeline[30] which included noise removal by principal component analysis (PCA) using the Marchenko–Pastur (MP) universal distribution,[31] followed by removal of Gibbs ringing artefacts using the method of local subvoxel shifts.[32] Afterward, we performed a correction for Eddy currents distortions and motion artefacts via FSL.[33] Data were collected with reversed phase-encoded blips, resulting in pairs of images with distortions going in opposite directions (PA). Mean PA field maps were down-sampled using FSL *flirt*[34] with an identity matrix and trilinear interpolation to match the voxel size of the mean AP b0 from DWI-HARDI images. From these pairs, the susceptibility-induced off-resonance field was estimated using a method similar to that described in Andersson et al.[35] as implemented in FSL,[36] and the two images were combined into a single corrected one. A brain mask was obtained using *dwi2mask*[37] at this point. Finally, a bias field correction was performed.[26]

2.7 | Processing

All b0 volumes were extracted from preprocessed HARDI images, which were then averaged into a single mean AP b0 volume. Coregistration of this mean volume from each participant to their anatomical T1w image was conducted using FreeSurfer's *bbregister*[34] to obtain a *.dat* registration file and then to apply it to the preprocessed HARDI image using *mri_vol2vol* with trilinear interpolation and to the brain mask using the same function with nearest-neighbour interpolation. We used the Accelerated Microstructure Imaging via Convex Optimization (AMICO) v1.2.10[38] implementation of NODDI.[11] Briefly, to extract its metrics, it is necessary to fit a NODDI model according to the data, using a hierarchical model (for more details, please refer to Daducci et al.),[38] to finally, extract its metrics (ICVF, ISOVF, and OD) within the brain mask voxels of each WM-ROI.

2.8 | WM regions of interest (ROIs)

We chose WM-ROIs corresponding to frontostriatal circuits based on a reported pathological brain target.[16] These circuits connect the following GM regions: lDLPFC, left caudate nucleus, substantia nigra, left globus pallidus, left thalamus, left and right vmPFC, and right AngG. To select ROI coordinates, we used the IIT Human Brain Atlas version 5.0[39] to select the following WM-ROIs: (1) left caudate nucleus and axial section through medulla (the closest in the atlas to substantia nigra) (*Caud2Medulla*, label 3785), (2) left caudate nucleus and left pallidum (*Caud2Palli*, label 3739), (3) left rostral middle frontal cortex (RMFC, the closest in atlas to lDLPFC) and left caudate nucleus (*DLPFC2Caud*, label 2637), (4) left RMFC and right medial orbitofrontal cortex (MOC, the closest in atlas to vmPFC) (*DLPFC2rvmPFC*, label 2662), (5) left RMFC and left thalamus (*DLPFC2Thal*, label 2636), (6) right inferior parietal cortex (IPC, the closest in atlas to right AngG) and right RMFC (*rAngG2rDLPFC*, label 5675), (7) left thalamus and axial section through medulla (*Thal2Medulla*, label 3685), (8) left thalamus and left pallidum (*Thal2Palli*, label 3639) and (9) left MOC and left RMFC (*vmPFC2DLPFC*, label 1326).

For each WM-ROI mask, we selected every voxel that was within the top 60 most probable fibre connections passing through that voxel by processing the file *IIT_WM_atlas_256.nii.gz* with *fslmaths*. For WM-ROI Masks 1 and 7 connecting to substantia nigra (axial section through medulla), an inferior manual deletion of all slices ($Z \leq 87$) was performed using *fsleyes*, because the WM mask extended inferiorly beyond substantia nigra when overlaying over *IIT-mean_t1_256.nii.gz*. A similar process was performed for WM-ROI masks (2 and 8) connecting to globus pallidus to delete all slices ($Z \leq 101$) because the WM mask extended inferiorly beyond globus pallidus.

To have a control tract, we used the same atlas to select a non-overlapping WM-ROI from the IIT_bundles, specifically CC_Forceps-Major_256 (forceps major of the corpus callosum: CCforcepsMajor). We used a custom mask of 10 lateral slices at each side of the midline plane slice excluding the most posterior 96 coronal slices. In this manner, the custom mask of the medial forceps major does not overlap with other used WM-ROIs nor any direct connection between the stimulation site and the occipital cortex. The medial forceps major was selected as it is a dense WM tract that is far from the stimulation site and should mostly contain fibres connecting the two occipital lobes.

To register WM-ROI masks into subjects' native spaces, we first performed a coregistration between FreeSurfer's *brain.mgz* and *IIT-mean_t1_256.nii.gz* by using *mri_robust_register*[40] to obtain an LTA registration file. The inverse of the LTA file was then used to warp with *mri_vol2vol* the WM-ROI masks into each subject's native space. These masks in native space were then used to obtain the mean NODDI metrics within each WM-ROI using R version 4.1.0 and *oro.nifti* version 0.11.0. Because of the proximity of the medial *CCforceps-Major* mask to the ventricles, any cerebrospinal fluid (CSF) voxel was explicitly excluded from the NODDI metric mean. Table 1 shows the descriptive statistics of these NODDI metrics across subjects.

2.9 | Statistical analyses

2.9.1 | Changes in WM microstructure 2 weeks after rTMS

Linear mixed-effects models were fitted to elucidate possible effects from active rTMS on frontostriatal WM tracts based on NODDI metrics while controlling for age and education years. The 30 fitted models were of the following structure:

$$NODDI_{ROI_i} = \beta_0 + \beta_1 \cdot weeks + \beta_2 \cdot rTMS[active] + \beta_3 \cdot age + \beta_4 \cdot educationyears + \beta_5 \cdot weeks \cdot rTMS[active],$$

in which $NODDI_{ROI_i}$ was the ICVF, ISOVF, or OD of each of the ten WM-ROIs. Tables 2-3, supplementary tables S1–S3 and Figures S1–S3 depict the estimates of β_5 from these 30 models (control WM-ROI models are depicted in Figure S1–S13).

2.9.2 | Baseline NODDI values as a predictor of clinical response to rTMS after 2 weeks

To investigate whether baseline NODDI metrics from frontostriatal circuits' WM tracts could predict clinical response to rTMS, several linear mixed-effects models were also fitted. The dependent variable was the clinical instrument score and the independent variables included the NODDI metric of each of the ten WM-ROIs, as shown in the following equation:

$$Score = \beta_0 + \beta_1 \cdot weeks + \beta_2 \cdot NODDI_{ROI_i} + \beta_3 \cdot rTMS[active] + \beta_4 \cdot age + \beta_5 \cdot educationyears + \beta_6 \cdot weeks \cdot NODDI_{ROI_i} + \beta_7 \cdot weeks \cdot rTMS[active] + \beta_8 \cdot NODDI_{ROI_i} \cdot rTMS[active] + \beta_9 \cdot NODDI_{ROI_i} \cdot age + \beta_{10} \cdot NODDI_{ROI_i} \cdot educationyears + \beta_{11} \cdot weeks \cdot NODDI_{ROI_i} \cdot rTMS[active],$$

in which *Score* was the score from VAS, CCQ-now, or BIS-11 and $NODDI_{ROI_i}$ the same as previously defined. Tables 2-3, supplementary tables S4–S12 and Figures S4–S12 depict the estimates of β_{11} from these 90 models (3 NODDI metrics × 10 WM-ROI × 3 scores from clinical instruments; control WM-ROI models are depicted in Figure S13).

We corrected *p* values using the false discovery rate or FDR method[41] on each of the 12 hypotheses families, each containing the 10 interactions of interest corresponding to the model of each WM-ROI. All statistical analyses were calculated using R version 4.1.0. Linear mixed models were performed using *lme4*, *effects*, *lmerTest* libraries, and *emmeans* for Cohen's effect size (*d*) calculated by estimated marginal means (emm).

3 | RESULTS

3.1 | Simulation of TMS electrical field

The simulation of the electric field indicated a maximal average electric-field norm (111.46 V/m) in the middle frontal gyrus (Figure 1).

3.2 | Changes in WM microstructure after 2 weeks rTMS

After 2 weeks, active rTMS showed significant increase in neurite density (ICVF or the density of axons and dendrites) compared with sham rTMS in WM tracts connecting lDLPFC with left vmPFC ($p = 0.013$, FDR = 0.065, $d = -0.278$; active-T0: 0.422 ± 0.135, active-T1: 0.461 ± 0.142) and right vmPFC ($p = 0.009$, FDR = 0.065, $d = -0.112$; active-T0: 0.451 ± 0.116, active-T1: 0.484 ± 0.126) (Table 2 and Figure 2), although it did not survive multiple comparisons at $q = 0.05$. Similarly, rTMS showed increasing in OD (or axon organization) in WM tracts connecting lDLPFC with left caudate nucleus ($p = 0.021$, FDR = 0.105, $d = -0.087$; active-T0: 0.41 ± 0.037, active-T1: 0.416 ± 0.035), left thalamus ($p = 0.045$, FDR = 0.150, $d = -0.489$; active-T0: 0.418 ± 0.03, active-T1: 0.42 ± 0.027) and left vmPFC ($p = 0.012$, FDR = 0.105, $d = 0.024$; active-T0: 0.294 ± 0.095, active-T1: 0.329 ± 0.096), without surviving multiple comparisons either (Table 2 and Figure 2). Here, we show that although all our changes were significant after 2 weeks, none survived our strict multiple comparisons and only the tracts connecting lDLPFC and vmPFC were near the threshold (FDR 5%) with a small effect size increase in the density of axons and dendrites after rTMS. The tract connecting lDLPFC and the left thalamus showed a medium effect size with an increase in axon organization. We did not find a correlation between changes in WM tracts and craving or impulsivity.

3.3 | Baseline NODDI values as a predictor of clinical outcome after rTMS

We found a greater reduction in craving VAS after 2 weeks of rTMS when baseline ICVF was low in WM tracts connecting the left caudate nucleus with substantia nigra ($p = 0.007$, FDR = 0.023, $d = 1.338$) and left pallidum ($p = 0.004$, FDR = 0.020, $d = 1.363$) and those connecting left thalamus with substantia nigra ($p = 0.012$, FDR = 0.030, $d = 1.321$) and left pallidum ($p = 0.002$, FDR = 0.020, $d = 1.430$) (Table 3 and Figure 3).

We found that BIS-11 responsiveness seemed to be predicted by a high baseline ISOVF or free water in WM connecting lDLPFC with left ($p = 0.015$, FDR = 0.150, $d = 1.364$) and right vmPFC ($p = 0.038$, FDR = 0.190, $d = 1.298$) (Table 3 and Figure 4A-B). None of these results concerning BIS-11 survived multiple comparisons.

Finally, we only found that baseline OD from WM connecting lDLPFC and right vmPFC, when high, predicted a greater decrease in BIS-11 ($p = 0.020$, FDR = 0.100, $d = 1.245$) (Table 3 and Figure 4C), without surviving multiple comparisons. These results suggest that low baseline axon and dendrite density of subcortical tracts predict changes in craving secondary to rTMS, with high effect sizes.

4 | DISCUSSION

Here, we investigated the effects of a 2-week treatment with rTMS over the lDLPFC on fronto-striato-thalamic WM microstructure in CUD patients, using multi-shell diffusion-weighted imaging and NODDI measures. We further evaluated the correlation of clinical changes in craving and impulsivity with baseline WM microstructure. Our results suggest that rTMS on lDLPFC induces WM microstructural changes (density of axons and dendrites and axon organization) in the lDLPFC–vmPFC and left subcortical connections after 2 weeks

TABLE 2 Coefficients of linear mixed-effects models' interaction (weeks:rTMS[active]) showing the effect of rTMS on NODDI metrics from frontostriatal circuits' white matter (WM) tracts.

WM-ROI	Estimate	Std. error	*df*	Effect size	*p* value	FDR[a]
Neurite density (ICVF)						
DLPFC2rvmPFC	0.034	0.012	42.36	−0.112	0.009[a]	0.065
vmPFC2DLPFC	0.038	0.015	42.31	−0.278	0.013[a]	0.065
Orientation dispersion (OD)						
DLPFC2Caud	0.009	0.004	40.65	−0.087	0.021[a]	0.105
DLPFC2Thal	0.006	0.003	40.68	−0.489	0.045[a]	0.150
vmPFC2DLPFC	0.027	0.010	41.91	0.024	0.012[a]	0.105

$NODDI_{ROI_i} = \beta_0 + \beta_1 \cdot weeks + \beta_2 \cdot rTMS[active] + \beta_3 \cdot age + \beta_4 \cdot educationyears + \beta_5 \cdot weeks \cdot rTMS[active]$

Abbreviations: DLPFC2Caud, WM connecting left rostral middle frontal cortex (RMFC) and left caudate nucleus; DLPFC2rvmPFC, WM connecting left RMFC and right medial orbitofrontal cortex (MOC); DLPFC2Thal, WM connecting left RMFC and left thalamus; vmPFC2DLPFC, WM connecting left MOC and left RMFC; WM-ROI, white matter region of interest; Std., standard; df; degrees of freedom; NODDI, neurite orientation dispersion and density imaging model; rTMS, repetitive transcranial magnetic stimulation, ICVF, intra-cellular volume fraction; ISOVF, isotropic volume fraction; OD, orientation dispersion.

[a]False discovery rate (FDR) adjustment was implemented with *p* values of their own metric, full values are found in Tables S1–S3.

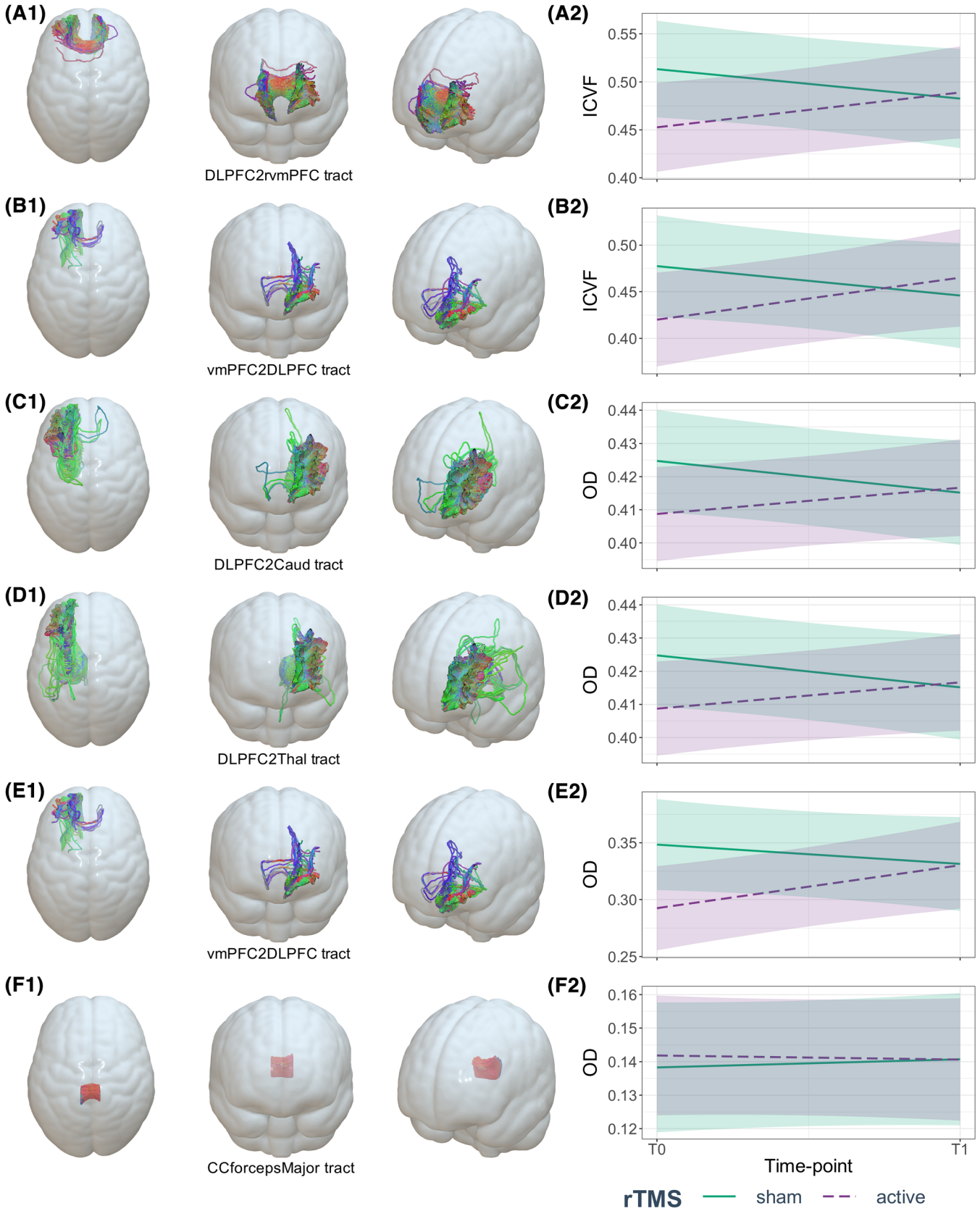

FIGURE 2 Legend on next page.

FIGURE 2 Effect of rTMS on neurite density (ICVF) and orientation dispersion (OD) from frontostriatal circuits' white matter (WM) tracts. (A2) Mean ICVF values at baseline and after 2 weeks of the WM connecting the left rostral middle frontal cortex and right medial orbitofrontal cortex (A1: DLPFC2rvmPFC), (B2) mean ICVF values at baseline and after 2 weeks of the WM connecting left medial orbitofrontal cortex and left rostral middle frontal cortex (B1: vmPFC2DLPFC), (C2) mean OD values at baseline and after 2 weeks of the WM connecting left rostral middle frontal cortex and left caudate nucleus (C1: DLPFC2Caud), (D2) mean OD values at baseline and after 2 weeks of the WM connecting left rostral middle frontal cortex and left thalamus (D1: DLPFC2Thal), (E2) mean OD values at baseline and after 2 weeks of the WM connecting left medial orbitofrontal cortex and left rostral middle frontal cortex (E1: vmPFC2DLPFC) and (F2) mean OD values at baseline and after 2 weeks of the WM from control ROI: forceps major of corpus callosum (F1: CCforcepsMajor).

TABLE 3 Coefficients of linear mixed-effects models' three-way interaction (weeks:NODDI:rTMS[active]) predicting a decrease in craving VAS/total BIS-11 using baseline NODDI metrics from frontostriatal circuits' WM tracts.

WM-ROI	Estimate	Std. error	*df*	Effect size	*p* value	FDR[a]
ICVF|Cocaine craving Visual Analogue Scale (VAS)						
Caud2Medulla	22.61	7.93	40.12	1.338	0.007[a]	0.023[a]
Caud2Palli	21.13	6.95	40.17	1.363	0.004[a]	0.020[a]
Thal2Medulla	16.30	6.17	40.07	1.321	0.012[a]	0.030[a]
Thal2Palli	21.92	6.61	40.13	1.430	0.002[a]	0.020[a]
ISOVF|Barratt Impulsivity Scale Version 11 (total BIS-11)						
DLPFC2rvmPFC	−49.81	23.25	39.63	1.298	0.038[a]	0.190
vmPFC2DLPFC	−103.78	40.96	40.51	1.364	0.015[a]	0.150
OD|Barratt Impulsivity Scale Version 11 (total BIS-11)						
DLPFC2rvmPFC	−56.76	23.43	39.80	1.245	0.020[a]	0.100
CCforcepsMajor	143.70	58.05	40.24	1.177	0.018[a]	0.100

$$Score = \beta_0 + \beta_1 \cdot weeks + \beta_2 \cdot NODDI_{ROI_i} + \beta_3 \cdot rTMS[active] + \beta_4 \cdot age + \beta_5 \cdot educationyears + \beta_6 \cdot weeks \cdot NODDI_{ROI_i} + \beta_7 \cdot weeks \cdot rTMS[active] + \beta_8 \cdot NODDI_{ROI_i} \cdot rTMS[active] + \beta_9 \cdot NODDI_{ROI_i} \cdot age + \beta_{10} \cdot NODDI_{ROI_i} \cdot educationyears + \beta_{11} \cdot weeks \cdot NODDI_{ROI_i} \cdot rTMS[active]$$

Abbreviations: Caud2Medulla, WM connecting left caudate nucleus and axial section through medulla; Caud2Palli, WM connecting left caudate nucleus and left pallidum; CCforcepsMajor, forceps major of corpus callosum (control WM); DLPFC2rvmPFC, WM connecting left rostral middle frontal cortex (RMFC) and right medial orbitofrontal cortex (MOC); Thal2Medulla, WM connecting left thalamus and axial section through medulla; Thal2Palli, WM connecting left thalamus and left pallidum; vmPFC2DLPFC, WM connecting left MOC and left RMFC; Std., standard; df; degrees of freedom; NODDI, neurite orientation dispersion and density imaging model; rTMS, repetitive transcranial magnetic stimulation.
[a]False discovery rate (FDR) adjustment was implemented with *p* values of their own metric, full values are found in Tables S4–S12.

of treatment. We also found that baseline WM microstructure predicted clinical response to rTMS treatment. The low density of axons and dendrites in left-caudate–substantia-nigra, left-caudate–left-pallidum, and left-thalamus–substantia-nigra, and left-thalamus–left-pallidum connections predicted greater craving reductions. While we found other significant results, none of these survived multiple comparisons correction. We still discuss these results due to their effect size and possible significance in rTMS.

Repeated TMS showed an effect in WM tracts after 2 weeks, evidenced by an increase in ICVF (axon/dendrite density) and OD (axon orientation), but not ISOVF (free water), in WM tracts connecting the lDLPFC to the vmPFC, left thalamus, and left caudate nucleus in the active group. We decided to discuss the ICVF result as it was significant at the individual level, with a moderate multiple comparisons non-significance, and a moderate to low effect size. These results may suggest a recovery of the integrity of prefrontal connections neurites with subcortical structures due to active rTMS as early as 2 weeks. The main mechanism of action proposed for rTMS in SUD treatment is that it activates dopamine (DA) function in the meso-cortico-limbic system and increases extracellular glutamate and DA concentrations.[8] This activation could trigger changes in dendritic spine density, neurotransmitter receptor expression, neuronal degeneration, and microglial activation which could explain the results in basal ganglia and PFC.[7,42,43] For example, rTMS may affect calcium and neurotransmission levels. Further, glutamate, GABA, and some monoamines like DA have been reported to increase after PFC rTMS, leading to dendritic spine enlargements through a signalling cascade.[7,42] DA is a critical neurotransmitter involved in synaptic plasticity in corticostriatal networks and in forming cue-induced craving; therefore, DA stimulation-induced release over the striatum has been proposed as the mechanism underlying the effects of rTMS in SUD patients.[8,42]

A previous study has found that rTMS can reach deep subcortical structures such as the amygdala through stimulation of cortical regions by cortico-subcortical structural connections.[44] Although the strongest stimulation effects remain at the scalp level, and rapidly attenuate as it crosses to brain tissue, the activations spread to other sites via axonal connections and the release of neurotransmitters, leading to deep structural and functional network changes.[8,45] Our results showed that active rTMS cortical effects in patients with CUD may have reached deep structures reflected by changes in NODDI

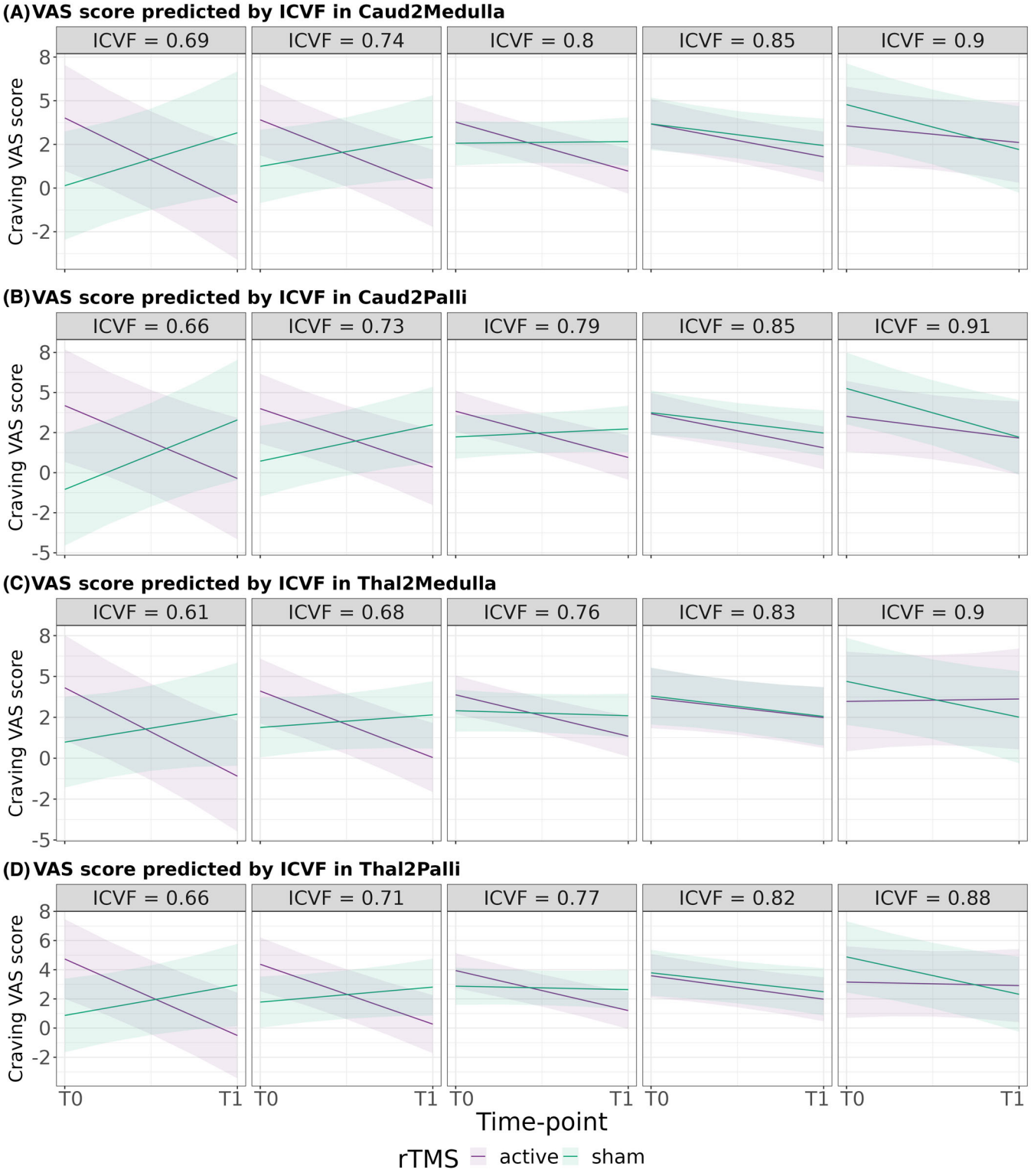

FIGURE 3 Prediction of craving VAS scores' change by the effect of rTMS according to baseline ICVF from frontostriatal circuits' WM tracts. (A) Prediction of craving VAS scores from different baseline ICVF values in WM connecting left caudate nucleus and axial section through medulla (Caud2Medulla), (B) prediction of craving VAS scores from different baseline ICVF values in WM connecting left caudate nucleus and left pallidum (Caud2Palli), (C) prediction of craving VAS scores from different baseline ICVF values in WM connecting left thalamus and axial section through medulla (Thal2Medulla) and (D) prediction of craving VAS scores from different baseline ICVF values in WM connecting left thalamus and left pallidum (Thal2Palli). VAS, craving Visual Analogue Scale; ICVF, neurite density index; T0, baseline time point; T1, after 2 weeks of rTMS protocol.

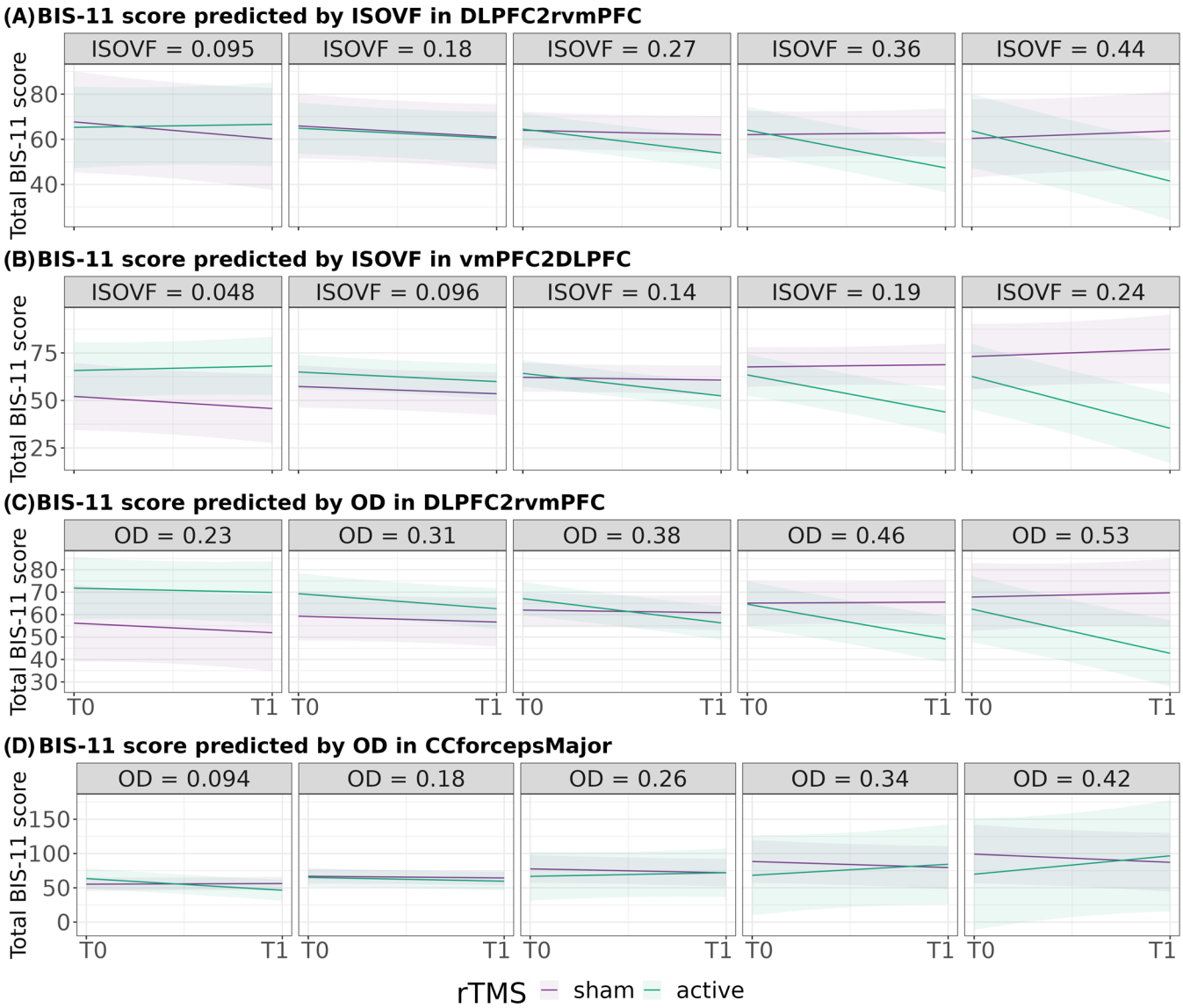

FIGURE 4 Prediction of total BIS-11 scores' change by the effect of rTMS according to ISOVF/OD from frontostriatal circuits' WM tracts. (A) Prediction of total BIS-11 scores from different baseline ISOVF values in WM connecting left rostral middle frontal cortex and right medial orbitofrontal cortex (DLPFC2rvmPFC), (B) prediction of total BIS-11 scores from different baseline ISOVF values in WM connecting left right medial orbitofrontal cortex and left rostral middle frontal cortex (vmPFC2DLPFC), (C) prediction of total BIS-11 scores from different baseline OD values in DLPFC2rvmPFC and (D) prediction of total BIS-11 scores from different baseline OD values in control ROI (CCforcepsMajor). BIS-11, Barratt Impulsivity Scale Version 11; ISOVF, cerebrospinal fluid volume fraction; OD, orientation dispersion; T0, baseline time point; T1, after 2 weeks of rTMS protocol.

metrics. Although we found these changes in WM tracts, they did not correlate to changes in craving or impulsivity.

Baseline ICVF of WM tracts connecting left caudate nucleus with substantia nigra and left pallidum and those connecting left thalamus with substantia nigra and left pallidum predicted a reduction in craving VAS after the rTMS treatment. These results survived multiple comparisons and were the most robust. This was not the case for ICVF from WM tracts connecting cortical with subcortical regions. On the contrary, baseline ISOVF predicted impulsivity responsiveness, in particular that from lDLPFC connections to left and right vmPFC. Similarly, baseline OD in one WM-ROI predicted BIS-11 responsiveness. However, these results did not survive multiple comparisons. We suggest that the initial state of WM integrity or the initial topology configuration is important for the rTMS outcome, or at least those patients had the highest changes after the therapy which may explain the higher effects. This may serve as an initial indication to select CUD patients that may more effectively benefit from this therapy. Prior studies have reported the association between subjective craving scores or impulsivity with diffusion metrics,[46,47] GM volumes,[48] and functional connectivity.[49] These studies have suggested a detrimental effect of cocaine use on the brain that could indicate the status of craving and impulsivity, supporting the idea of WM-GM

integrity as an indicator of CUD severity and the guidance to achieving effective recovery.

Previous studies have found associations between repetitive stimulation over the DLPFC and the mPFC with improvements in executive functions and reward functions, as well as reduction of craving/drug consumption in patients with CUD.[50,51] Additionally, rTMS applied to this region has been shown to induce microstructural changes in patients with depression. Changes include alterations in free water, fractional anisotropy, and radial diffusivity within frontal-fibre bundles, which appear to be associated with therapeutic improvement.[12,52,53] These results indicate that rTMS-induced modulation may be mediated by neurotransmitter systems (i.e., the dopaminergic, GABA, and glutamatergic pathways), metabolism, cell survival, and neural activity modulation. These findings do not only strengthen the potential of TMS as a therapeutic tool but also provide background to explain the mechanisms through which structural changes occur and relate to disease pathophysiology, as has been suggested previously.[7,54]

The prediction of craving outcome based on the state of microstructure prior to stimulations could suggest that greater neurite integrity will result in better rTMS clinical outcomes, which is in line with previous studies that have found associations between WM-GM baseline integrity with better longitudinal clinical outcomes that can inform if patients will relapse or remain in drug abstinent.[55] This idea may be supported by the low effect size we found for NODDI changes, but high for NODDI as a predictor. This may imply that irrespective of the induced changes, the initial integrity state has the highest impact on how rTMS modulates brain circuits and on the possible success of clinical outcomes.

One of the main limitations of the present work concerns the longitudinal course, which is restricted to a single time point, only after 2 weeks. The results of which could be statistically confirmed with continued use of rTMS in the months of patient follow-up, as well as being extended to other regions. Even so, finding significant changes at 2 weeks suggests rTMS affects WM structure from the first day of stimulation. According to previous clinical disorders studies, ICVF is decreased with axonal degeneration, axonal loss, and demyelination processes, while OD decreasing reflects a selective loss of crossing fibres, axonal regrowth, and reduced axonal dispersion.[10] However, other researchers have found inconsistent results in terms of NODDI values directionality and the biological interpretation of it.[10,13] In this context, validation of NODDI values in terms of biological meaning would help to elucidate the current results. Discussion regarding the clinical sample variability and composition here used can be found in Garza-Villarreal et al.[16]

5 | CONCLUSION

In conclusion, here showed changes in neurite microstructure in connections between frontostriatal circuits regions, after active rTMS stimulation in CUD, suggesting a plasticity-induced recovery of the integrity of these connections. The prediction of the craving state based on baseline NODDI values before the onset of rTMS suggests that rTMS efficacy depends on the consumption-related integrity state of the underlying microstructure. Our results highlight rTMS as a potential therapeutic tool in the treatment of CUD, due to its ability to modulate altered brain microstructure by cocaine use, as well as the relevance of NODDI for tracing drug/treatment responsiveness.

AUTHOR CONTRIBUTIONS

Jalil Rasgado-Toledo: Formal analysis; software; methodology; visualization; writing—original draft. **Victor Issa-Garcia:** Formal analysis; software; methodology; writing—original draft. **Ruth Alcalá-Lozano:** Funding acquisition; investigation; supervision; project administration; resources; writing—review and editing. **Eduardo A. Garza-Villarreal:** Conceptualization; design; funding acquisition; investigation; supervision; project administration; resources; writing—review and editing. **Gabriel González-Escamilla:** Conceptualization; methodology; investigation; supervision; writing—review and editing.

ACKNOWLEDGEMENTS

The study was supported by public funds CONACYT FOSISS (0260971), CONACYT (253072), and PAPIIT-UNAM (IA202120). Victor Issa-Garcia and Eduardo A. Garza-Villarreal would like to thank Dirección General de Calidad y Educación en Salud, Secretaría de Salud, México, for the scholarship support provided to Victor. We also thank the Laboratorio Nacional de Visualización Científica Avanzada (LAVIS) for the use of their computer cluster and the Laboratorio Nacional de Imagenología por Resonancia Magnética (LANIREM). Gabriel González-Escamilla is supported by a grant from the German Research Foundation (DFG; CRC-TR-128) and received funds from the DFG (GO 3493/1-1). Jalil Rasgado-Toledo is a doctoral student from the Programa de Doctorado en Ciencias Biomédicas, Universidad Nacional Autónoma de México (UNAM) and received a fellowship 858667 from CONACYT.

CONFLICT OF INTEREST STATEMENT

None.

DATA AVAILABILITY STATEMENT

The MRI dataset can be found at https://openneuro.org/datasets/ds003037/. Clinical and cognitive measures are available in Zenodo https://doi.org/10.5281/zenodo.7126853.

ETHICS STATEMENT

Data were obtained from a clinical trial conducted at the Clinical Research Division of the National Institute of Psychiatry in Mexico City, Mexico, that was approved by the Institutional Ethics Research Committee (CEI/C/070/2016). Clinical trial registration: registered at ClinicalTrials.gov (NCT02986438).

CODE AVAILABILITY

For the code analysis presented here, please check https://jalilrt.github.io/NODDI-changes-by_rTMS-in_CUD/.

ORCID

Jalil Rasgado-Toledo https://orcid.org/0000-0001-5216-7177
Victor Issa-Garcia https://orcid.org/0000-0002-9596-988X
Ruth Alcalá-Lozano https://orcid.org/0000-0001-7720-2434
Eduardo A. Garza-Villarreal https://orcid.org/0000-0003-1381-8648

REFERENCES

1. United Nations Office on Drugs and Crime. *World Drug Report 2021 (Set of 5 Booklets)*. United Nations; 2022. https://play.google.com/store/books/details?id=LMNdEAAAQBAJ
2. Volkow ND, Koob GF, McLellan AT. Neurobiologic advances from the brain disease model of addiction. *N Engl J Med*. 2016;374(4):363-371. doi:10.1056/NEJMra1511480
3. Nestler E. The neurobiology of cocaine addiction. *Science & Practice Perspectives*. 2005;3(1):4-10. doi:10.1151/spp05314
4. Hirsiger S, Hänggi J, Germann J, et al. Longitudinal changes in cocaine intake and cognition are linked to cortical thickness adaptations in cocaine users. *Neuroimage Clin*. 2019;21:101652. doi:10.1016/j.nicl.2019.101652
5. Kampman KM. The treatment of cocaine use disorder. *Sci Adv*. 2019;5(10):eaax1532. doi:10.1126/sciadv.aax1532
6. Steele VR, Maxwell AM. Treating cocaine and opioid use disorder with transcranial magnetic stimulation: a path forward. *Pharmacol Biochem Behav*. 2021;209:173240. doi:10.1016/j.pbb.2021.173240
7. Moretti J, Rodger J. A little goes a long way: neurobiological effects of low intensity rTMS and implications for mechanisms of rTMS. *Curr Res Neurobiol*. 2022;3:100033. doi:10.1016/j.crneur.2022.100033
8. Diana M, Raij T, Melis M, Nummenmaa A, Leggio L, Bonci A. Rehabilitating the addicted brain with transcranial magnetic stimulation. *Nat Rev Neurosci*. 2017;18(11):685-693. doi:10.1038/nrn.2017.113
9. Nazeri A, Schifani C, Anderson JAE, Ameis SH, Voineskos AN. In vivo imaging of gray matter microstructure in major psychiatric disorders: opportunities for clinical translation. *Biol Psychiatry Cogn Neurosci Neuroimaging*. 2020;5(9):855-864. doi:10.1016/j.bpsc.2020.03.003
10. Kamiya K, Hori M, Aoki S. NODDI in clinical research. *J Neurosci Methods*. 2020;346:108908. doi:10.1016/j.jneumeth.2020.108908
11. Zhang H, Schneider T, Wheeler-Kingshott CA, Alexander DC. NODDI: practical in vivo neurite orientation dispersion and density imaging of the human brain. *Neuroimage*. 2012;61(4):1000-1016. doi:10.1016/j.neuroimage.2012.03.072
12. Ning L, Rathi Y, Barbour T, Makris N, Camprodon JA. White matter markers and predictors for subject-specific rTMS response in major depressive disorder. *J Affect Disord*. 2022;299:207-214. doi:10.1016/j.jad.2021.12.005
13. Kraguljac NV, Guerreri M, Strickland MJ, Zhang H. Neurite orientation dispersion and density imaging in psychiatric disorders: a systematic literature review and a technical note. *Biol Psychiatry Glob Open Sci*. 2022;3(1):10-21. doi:10.1016/j.bpsgos.2021.12.012
14. Rasgado-Toledo J, Shah A, Ingalhalikar M, Garza-Villarreal EA. Neurite orientation dispersion and density imaging in cocaine use disorder. *Prog Neuropsychopharmacol Biol Psychiatry*. 2022;113:110474. doi:10.1016/j.pnpbp.2021.110474
15. Angeles-Valdez D, Rasgado-Toledo J, Villicaña V, et al. The Mexican dataset of a repetitive transcranial magnetic stimulation clinical trial on cocaine use disorder patients: SUDMEX TMS. *bioRxiv*. 2023. doi:10.1101/2023.06.21.23291661
16. Garza-Villarreal EA, Alcala-Lozano R, Fernandez-Lozano S, et al. Clinical and functional connectivity outcomes of 5-Hz repetitive transcranial magnetic stimulation as an add-on treatment in cocaine use disorder: a double-blind randomized controlled trial. *Biol Psychiatry Cogn Neurosci Neuroimaging*. 2021;6(7):745-757. doi:10.1016/j.bpsc.2021.01.003
17. Sayette MA, Shiffman S, Tiffany ST, Niaura RS, Martin CS, Schadel WG. The measurement of drug craving. *Addiction*. 2000;95(8s2):189-210. doi:10.1046/j.1360-0443.95.8s2.8.x
18. Tiffany ST, Singleton E, Haertzen CA, Henningfield JE. The development of a cocaine craving questionnaire. *Drug Alcohol Depend*. 1993;34(1):19-28. doi:10.1016/0376-8716(93)90042-o
19. Marín-Navarrete R, Mejía-Cruz D, Templos-Nuñez L, et al. Validation of a cocaine craving questionnaire (CCQ-G) in Mexican population. *Salud Ment*. 2011;34(6):491-496. https://www.medigraphic.com/cgi-bin/new/resumenI.cgi?IDARTICULO=32347
20. Patton JH, Stanford MS, Barratt ES. Factor structure of the Barratt impulsiveness scale. *J Clin Psychol*. 1995;51(6):768-774. doi:10.1002/1097-4679(199511)51:63.0.co;2-1
21. Oquendo MA, Baca-García E, Graver R, Morales M, Montalvan V, Mann JJ. Spanish adaptation of the Barratt Impulsiveness Scale (BIS-11). *Eur Psychiatry*. 2001;15(3):147-155. https://psycnet.apa.org/fulltext/2001-18816-003.pdf
22. Saturnino GB, Puonti O, Nielsen JD, Antonenko D, Madsen KH, Thielscher A. SimNIBS 2.1: a comprehensive pipeline for individualized electric field modelling for transcranial brain stimulation. In: Makarov S, Horner M, Noetscher G, eds. *Brain and Human Body Modeling: Computational Human Modeling at EMBC 2018*. Springer; 2019. doi:10.1007/978-3-030-21293-3
23. Nielsen JD, Madsen KH, Puonti O, et al. Automatic skull segmentation from MR images for realistic volume conductor models of the head: assessment of the state-of-the-art. *Neuroimage*. 2018;174:587-598. doi:10.1016/j.neuroimage.2018.03.001
24. Esteban O, Markiewicz CJ, Blair RW, et al. fMRIPrep: a robust preprocessing pipeline for functional MRI. *Nat Methods*. 2019;16(1):111-116. doi:10.1038/s41592-018-0235-4
25. Gorgolewski K, Burns CD, Madison C, et al. Nipype: a flexible, lightweight and extensible neuroimaging data processing framework in Python. *Front Neuroinf*. 2011;5:13. doi:10.3389/fninf.2011.00013
26. Tustison NJ, Avants BB, Cook PA, et al. N4ITK: improved N3 bias correction. *IEEE Trans Med Imaging*. 2010;29(6):1310-1320. doi:10.1109/TMI.2010.2046908
27. Dale AM, Fischl B, Sereno MI. Cortical surface-based analysis. I. Segmentation and surface reconstruction. *Neuroimage*. 1999;9(2):179-194. doi:10.1006/nimg.1998.0395
28. Klein A, Ghosh SS, Bao FS, et al. Mindboggling morphometry of human brains. *PLoS Comput Biol*. 2017;13(2):e1005350. doi:10.1371/journal.pcbi.1005350
29. Tournier JD, Smith R, Raffelt D, et al. MRtrix3: a fast, flexible and open software framework for medical image processing and visualisation. *Neuroimage*. 2019;202:116137. doi:10.1016/j.neuroimage.2019.116137
30. Bange M, Gonzalez-Escamilla G, Lang NSC, et al. Gait abnormalities in Parkinson's disease are associated with extracellular free-water characteristics in the substantia nigra. *J Parkinsons Dis*. 2022;12(5):1575-1590. doi:10.3233/JPD-223225
31. Veraart J, Fieremans E, Novikov DS. Diffusion MRI noise mapping using random matrix theory. *Magn Reson Med*. 2016;76(5):1582-1593. doi:10.1002/mrm.26059
32. Kellner E, Dhital B, Kiselev VG, Reisert M. Gibbs-ringing artifact removal based on local subvoxel-shifts. *Magn Reson Med*. 2016;76(5):1574-1581. doi:10.1002/mrm.26054
33. Andersson JLR, Sotiropoulos SN. An integrated approach to correction for off-resonance effects and subject movement in diffusion MR imaging. *Neuroimage*. 2016;125:1063-1078. doi:10.1016/j.neuroimage.2015.10.019
34. Greve DN, Fischl B. Accurate and robust brain image alignment using boundary-based registration. *Neuroimage*. 2009;48(1):63-72. doi:10.1016/j.neuroimage.2009.06.060

35. Andersson JLR, Skare S, Ashburner J. How to correct susceptibility distortions in spin-echo echo-planar images: application to diffusion tensor imaging. *Neuroimage*. 2003;20(2):870-888. doi:10.1016/S1053-8119(03)00336-7
36. Smith SM, Jenkinson M, Woolrich MW, et al. Advances in functional and structural MR image analysis and implementation as FSL. *Neuroimage*. 2004;23(Suppl 1):S208-S219. doi:10.1016/j.neuroimage.2004.07.051
37. Dhollander T, Raffelt D, Connelly A. Unsupervised 3-tissue response function estimation from single-shell or multi-shell diffusion MR data without a co-registered T1 image. In: *ISMRM Workshop on Breaking the Barriers of Diffusion MRI*. Vol.5. ISMRM; 2016. https://www.researchgate.net/profile/Thijs-Dhollander/publication/307863133_Unsupervised_3-tissue_response_function_estimation_from_single-shell_or_multi-shell_diffusion_MR_data_without_a_co-registered_T1_image/links/57cfb5c708ae83b374623e5a/Unsupervised-3-tissue-response-function-estimation-from-single-shell-or-multi-shell-diffusion-MR-data-without-a-co-registered-T1-image.pdf
38. Daducci A, Canales-Rodríguez EJ, Zhang H, Dyrby TB, Alexander DC, Thiran JP. Accelerated Microstructure Imaging via Convex Optimization (AMICO) from diffusion MRI data. *Neuroimage*. 2015;105:32-44. doi:10.1016/j.neuroimage.2014.10.026
39. Zhang S, Arfanakis K. Evaluation of standardized and study-specific diffusion tensor imaging templates of the adult human brain: template characteristics, spatial normalization accuracy, and detection of small inter-group FA differences. *NeuroImage*. 2018;172:40-50. doi:10.1016/j.neuroimage.2018.01.046
40. Reuter M, Rosas HD, Fischl B. Highly accurate inverse consistent registration: a robust approach. *Neuroimage*. 2010;53(4):1181-1196. doi:10.1016/j.neuroimage.2010.07.020
41. Benjamini Y, Hochberg Y. Controlling the false discovery rate: a practical and powerful approach to multiple testing. *J Royal Stat Soc Series B (Methodological)*. 1995;57(1):289-300. doi:10.1111/j.2517-6161.1995.tb02031.x
42. Moretti J, Poh EZ, Rodger J. rTMS-induced changes in glutamatergic and dopaminergic systems: relevance to cocaine and methamphetamine use disorders. *Front Neurosci*. 2020;14:137. doi:10.3389/fnins.2020.00137
43. Gay A, Cabe J, De Chazeron I, et al. Repetitive transcranial magnetic stimulation (rTMS) as a promising treatment for craving in stimulant drugs and behavioral addiction: a meta-analysis. *J Clin Med Res*. 2022;11(3):624. doi:10.3390/jcm11030624
44. Sydnor VJ, Cieslak M, Duprat R, et al. Cortical-subcortical structural connections support transcranial magnetic stimulation engagement of the amygdala. *Sci Adv*. 2022;8(25):eabn5803. doi:10.1126/sciadv.abn5803
45. Klooster DCW, Ferguson MA, Boon PAJM, Baeken C. Personalizing repetitive transcranial magnetic stimulation parameters for depression treatment using multimodal neuroimaging. *Biol Psychiatry Cogn Neurosci Neuroimaging*. 2022;7(6):536-545. doi:10.1016/j.bpsc.2021.11.004
46. Gaudreault PO, King SG, Malaker P, Alia-Klein N, Goldstein RZ. Whole-brain white matter abnormalities in human cocaine and heroin use disorders: association with craving, recency, and cumulative use. *Mol Psychiatry*. 2022;28(2):780-791. doi:10.1038/s41380-022-01833-y
47. Moeller FG, Hasan KM, Steinberg JL, et al. Reduced anterior corpus callosum white matter integrity is related to increased impulsivity and reduced discriminability in cocaine-dependent subjects: diffusion tensor imaging. *Neuropsychopharmacology*. 2005;30(3):610-617. doi:10.1038/sj.npp.1300617
48. Ersche KD, Barnes A, Jones PS, Morein-Zamir S, Robbins TW, Bullmore ET. Abnormal structure of frontostriatal brain systems is associated with aspects of impulsivity and compulsivity in cocaine dependence. *Brain*. 2011;134(Pt 7):2013-2024. doi:10.1093/brain/awr138
49. Hu Y, Salmeron BJ, Gu H, Stein EA, Yang Y. Impaired functional connectivity within and between frontostriatal circuits and its association with compulsive drug use and trait impulsivity in cocaine addiction. *JAMA Psychiatry*. 2015;72(6):584-592. doi:10.1001/jamapsychiatry.2015.1
50. Protasio MIB, Da Silva JPL, Machado S, Chagas SV, Murillo-Rodriguez E, Cruz MS. The effects of repetitive transcranial magnetic stimulation in reducing cocaine craving and use. *Addict Disord Their Treat*. 2019;18(4):212-222. doi:10.1097/adt.0000000000000169
51. Zhang JJQ, Fong KNK, Ouyang R, Siu AMH, Kranz GS. Effects of repetitive transcranial magnetic stimulation (rTMS) on craving and substance consumption in patients with substance dependence: a systematic review and meta-analysis. *Addiction*. 2019;114(12):2137-2149. doi:10.1111/add.14753
52. Schiena G, Franco G, Boscutti A, Delvecchio G, Maggioni E, Brambilla P. Connectivity changes in major depressive disorder after rTMS: a review of functional and structural connectivity data. *Epidemiol Psychiatr Sci*. 2021;30:e59. doi:10.1017/s2045796021000482
53. Fu Y, Long Z, Luo Q, et al. Functional and structural connectivity between the left dorsolateral prefrontal cortex and insula could predict the antidepressant effects of repetitive transcranial magnetic stimulation. *Front Neurosci*. 2021;15:645936. doi:10.3389/fnins.2021.645936
54. Aceves-Serrano L, Neva JL, Doudet DJ. Insight into the effects of clinical repetitive transcranial magnetic stimulation on the brain from positron emission tomography and magnetic resonance imaging studies: a narrative review. *Front Neurosci*. 2022;16:787403. doi:10.3389/fnins.2022.787403
55. Moeller SJ, Paulus MP. Toward biomarkers of the addicted human brain: using neuroimaging to predict relapse and sustained abstinence in substance use disorder. *Prog Neuropsychopharmacol Biol Psychiatry*. 2018;80(Pt B):143-154. doi:10.1016/j.pnpbp.2017.03.003

SUPPORTING INFORMATION

Additional supporting information can be found online in the Supporting Information section at the end of this article.

How to cite this article: Rasgado-Toledo J, Issa-Garcia V, Alcalá-Lozano R, Garza-Villarreal EA, González-Escamilla G. Cortical and subcortical microstructure integrity changes after repetitive transcranial magnetic stimulation therapy in cocaine use disorder and relates to clinical outcomes. *Addiction Biology*. 2024;29(2):e13381. doi:10.1111/adb.13381